INTERNATIONAL JOURNAL OF CLIMATOLOGY
Int. J. Climatol. **36**: 3175–3190 (2016)
Published online 9 November 2015 in Wiley Online Library
(wileyonlinelibrary.com) DOI: 10.1002/joc.4545

RMetS
Royal Meteorological Society

Influence of winter season climate variability on snow–precipitation ratio in the western United States

Mohammad Safeeq,[a,b]* Shraddhanand Shukla,[c] Ivan Arismendi,[d] Gordon E. Grant,[e] Sarah L. Lewis[f] and Anne Nolin[f]

[a] *Sierra Nevada Research Institute, University of California, Merced, CA, USA*
[b] *USDA Forest Service, PSW Research Station, Fresno, CA, USA*
[c] *Department of Geography, University of California, Santa Barbara, CA, USA*
[d] *Department of Fisheries and Wildlife, Oregon State University, Corvallis, OR, USA*
[e] *USDA Forest Service, PNW Research Station, Corvallis, OR, USA*
[f] *College of Earth, Ocean and Atmospheric Sciences, Oregon State University, Corvallis, OR, USA*

ABSTRACT: In the western United States, climate warming poses a unique threat to water and snow hydrology because much of the snowpack accumulates at temperatures near 0 °C. As the climate continues to warm, much of the region's precipitation is expected to switch from snow to rain, causing flashier hydrographs, earlier inflow to reservoirs, and reduced spring and summer snowpack. This study investigates historical variability in snow to precipitation proportion (S_f) and maps areas in the western United States that have demonstrated higher S_f sensitivity to warming in the past. Projected changes in S_f under 1.1, 1.8, and 3.0 °C future warming scenarios are presented in relation to historical variability and sensitivity. Our findings suggest that S_f in this region has primarily varied based on winter temperature rather than precipitation. The difference in S_f between cold and warm winters at low- and mid-elevations during 1916–2003 ranged from 31% in the Pacific Northwest to 40% in the California Sierra Nevada. In contrast, the difference in S_f between wet and dry winters was statistically not significant. Overall, in the northern Sierra, Klamath, and western slopes of the Cascade Mountains Ranges, S_f was most sensitive to temperature where winter temperature ranged between −5 to 5 °C. Results from our trend analysis show a regional shift in both S_f and signal-to-noise ratios during 1960–2003 as compared with 1916–2003. Our findings indicate that natural variability in S_f over 1916–2003 across all regions except for the Great Basin most closely resembles the projected 2040-warming scenario (+1.8 °C).

KEY WORDS snow fraction; climate warming; signal-to-noise ratio; trend analysis; western United States

Received 16 March 2015; Revised 28 September 2015; Accepted 29 September 2015

1. Introduction

Mountain snowpacks in the western United States serve as the primary source of spring and summer runoff, which supports ecosystems as well as agriculture, industry, and urban uses. Declines in streamflow magnitude (Lins and Slack, 1999; Luce and Holden, 2009), earlier streamflow timing (Stewart *et al.*, 2005), and altered flood risk (Hamlet and Lettenmaier, 2007) have been reported for this region, all of which are primarily attributed to changes in snowpack. Significant reductions in snowpack accumulation and earlier snowmelt have been attributed at least in part to anthropogenic climate warming (Barnett *et al.*, 2008; Hidalgo *et al.*, 2009). Continuing warming trends in mid-latitude areas (Intergovernmental Panel on Climate Change (IPCC), 2007a, 2007b; Adam *et al.*, 2009) would only intensify changes in snow accumulation and melt rate across the western United States (Gleick, 1987; Lettenmaier and Gan, 1990; Dettinger *et al.*, 2004; Knowles and Cayan, 2004; Stewart *et al.*, 2004).

As temperatures continue to warm, much of this region is expected to experience a shift from solid to liquid phase precipitation (Knowles *et al.*, 2006). More precipitation falling as rain instead of snow, and consequently a lower total snowfall to precipitation ratio (hereinafter referred to as snow fraction, S_f), would affect total snow accumulation and the timing of snowmelt and runoff regimes, potentially leading to higher winter floods and lower flow in late spring and summer (Safeeq *et al.*, 2013, 2015). In any given region, however, changes in S_f would depend on overall climatic regime as well as the corresponding changes in temperature and precipitation. Specifically, areas where snow accumulates at temperatures near 0 °C, also known as the transient snow zone, are more vulnerable to warming than areas with snow accumulating at colder temperatures (Hamlet *et al.*, 2005; Nolin and Daly, 2006; Sproles *et al.*, 2013).

The transient snow zone is of particular hydrologic interest, not only from the perspective of climate change but also for its role in generating large floods through rain-on-snow events (Harr, 1981; Christner and Harr, 1982; Marks *et al.*, 1998; O'Connor and Costa, 2003; Surfleet and Tullos, 2012). To date, identification of the

* Correspondence to: M. Safeeq, Sierra Nevada Research Institute, University of California, 5200 N Lake Road, Merced, CA 95343, USA. E-mail: msafeeq@ucmerced.edu

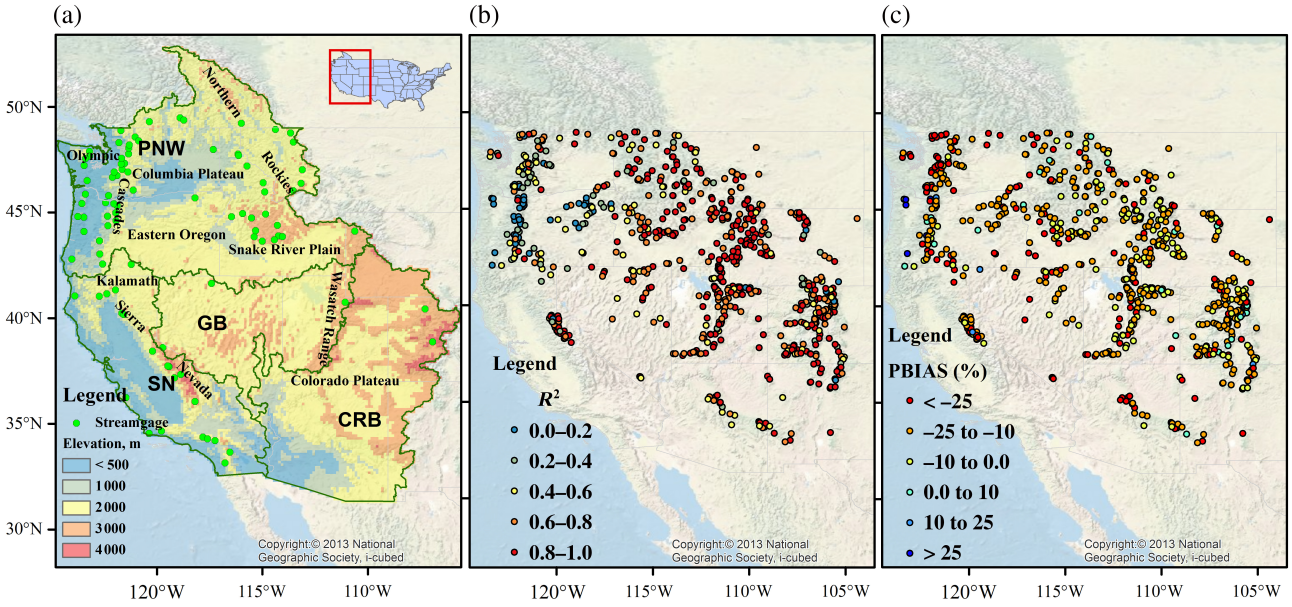

Figure 1. (a) Drainage boundary and topographic characteristics of the four study regions: Sierra Nevada (SN), Colorado River basin (CRB), Great basin (GB), Columbia River, and Pacific Northwest coastal basins (PNW); (b) coefficient of determination (R^2) and (c) percent bias (negative PBIAS = underestimation, positive PBIAS = overestimation) between observed snow water equivalent and those empirically derived from temperature and precipitation using Equation (1).

transient snow zone has always been based on elevation (Christner and Harr, 1982; Harr, 1986; Surfleet and Tullos, 2012) and/or temperature thresholds (Hamlet and Lettenmaier, 2007; Jefferson, 2011). This is mainly due to the limited spatiotemporal coverage and record length of directly relevant climatological [i.e. snow water equivalent (SWE), precipitation, wind speed, and temperature] measurements (Hamlet *et al.*, 2005). Availability of high-quality spatially distributed gridded meteorological data has improved our ability to analyze changes in snowpack and controls in a more spatially explicit fashion (Hamlet *et al.*, 2005; Nolin and Daly, 2006; Das *et al.*, 2009), as opposed to only a point-based analysis (Karl *et al.*, 1993; Frei *et al.*, 1999; Mote *et al.*, 2005; Knowles *et al.*, 2006; Feng and Hu, 2007).

Previous work has shown decreasing trends in snowpack in the western United States (Frei *et al.*, 1999; Mote *et al.*, 2005; Brown and Mote, 2009; Abatzoglou, 2011; Harpold *et al.*, 2012; Rupp *et al.*, 2013). The relative contributions of changing temperature and precipitation on the snow fraction (Hamlet *et al.*, 2005; Knowles *et al.*, 2006; Feng and Hu, 2007) and on hydrologic drought have also been documented (Mao *et al.*, 2015; Shukla *et al.*, 2015). To our knowledge, there have been no studies showing the historical spatiotemporal variability in S_f and how this relates to past and potential future trends. Studies showing monotonic trends in S_f provide only a partial view of future snowpacks, and cannot clarify whether, on average, future snowpacks would be smaller than extreme years in the past, or stay within the range of historic variability. The answer to this question has direct implications for water use, especially for reservoir operations in the western United States. Insight into signal (monotonic trends) to noise (historical variability) ratios would be useful for effectively managing water resources and aquatic ecosystems. Our objectives here are to: (1) quantify the historical variability in S_f during extreme years and examine how this relates to future climate warming in a spatially explicit fashion; (2) quantify the sensitivity of S_f to temperature as evidenced in the historical record; and (3) determine the spatiotemporal variability in S_f trends over the western United States.

2. Datasets and analyses

2.1. Precipitation and temperature dataset

We used gridded, 1/8th degree spatial resolution, daily precipitation, and temperature datasets for 1916–2003 to compute S_f after dividing the study domain into four regions: (a) the California Sierra Nevada (SN); (b) the Colorado River Basin (CRB); (c) the Great Basin (GB); and (d) the Columbia River Basin and coastal Oregon and Washington (PNW) (Figure 1(a)). These gridded datasets were developed using precipitation and temperature observations from the National Climatic Data Service's Cooperative Observer (Coop) network (Hamlet and Lettenmaier, 2005). Using gridded temperature and precipitation datasets for estimating S_f as opposed to using direct temperature and precipitation observations from weather stations has both advantages and disadvantages. The advantage of using gridded meteorological datasets is that they provide spatially and temporally consistent meteorological conditions at places where direct observations are sparse (Hamlet *et al.*, 2005). The main disadvantage is that gridded datasets are derived through interpolation of available

station data and subjected to a number of potential inaccuracies and errors that can propagate to the estimates of S_f or any other derived spatial data. These errors can be introduced by an irregularly spaced underlying station network, inaccurate and missing observations, and the interpolation method used. In many mountainous regions, such as the western United States, the network of meteorological stations at middle and high altitudes is sparse. In addition, changes in number of functioning weather stations and their location, instrumentation, and land use may cause inhomogeneity in observed temperature and precipitation that can propagate into gridded datasets.

Nevertheless, the gridded datasets used in this study were specifically developed to overcome some of the aforementioned issues and facilitate long-term trend analyses of simulated hydrologic variables (Hamlet and Lettenmaier, 2005). The raw temperature and precipitation data from Coop stations were first screened for inaccuracies and then gridded using 4 and 15 nearest neighbors for temperature and precipitation, respectively. A higher number of nearest neighbors were used for precipitation to prevent sharp discontinuities in the gridded data as a result of the relatively low station density. After the gridding process, both temperature and precipitation were subjected to temporal and altitudinal adjustments to account for changes in number and locations of Coop stations over time as well as to deal with any biases associated with the sparse station network at middle and higher elevations. Detailed description of the data and gridding algorithms can be found in Hamlet and Lettenmaier (2005).

2.2. Snow fraction

Daily precipitation (P) and average temperature values (calculated as the arithmetic mean of daily maximum and minimum temperatures) were used to calculate the annual winter season (November-March) S_f and average wet day (daily precipitation > 0) temperature (T_{w_avg}). Our definition of winter season is consistent with Knowles *et al.* (2006), who reported 80% of snowfall occurring during this season. Annual S_f for each grid cell was determined after partitioning P into rain and snow using the linear empirical relationship developed by the United States Army Corps of Engineers (1956). Sproles *et al.* (2013) evaluated additional computationally complex rain and snow partitioning algorithms, but the results were identical. The snowfall equivalent (SFE) (mm), defined as the amount of P reaching the ground as snow, was calculated as follows:

$$\mathrm{SFE} = \begin{cases} P, & T_{w\_avg} \le \mathrm{TS} \\ 0, & T_{w\_avg} \ge \mathrm{TR} \\ \frac{1}{\mathrm{TR}-\mathrm{TS}} \times \left(\mathrm{TR} - T_{w\_avg}\right) \times P & \mathrm{TS} < T_{w\_avg} < \mathrm{TR} \end{cases} \quad (1)$$

where, T_{w_avg} is the average daily air temperature (°C), TR is the temperature above which all precipitation fell as rain, TS is the temperature below which all precipitation fell as snow, and P is the total daily precipitation (mm day^{-1}).

The annual winter season S_f was calculated as:

$$S_f\,(\%) = \frac{\sum_{i=1}^{n} \mathrm{SFE}_i}{\sum_{i=1}^{n} \mathrm{P}_i} \times 100 \quad (2)$$

where n was the last day of the winter season. The value of S_f ranged between 0 (all rain) and 100% (all snow).

We acknowledge the limitation of an empirically derived SFE based on a temperature threshold alone, due primarily to the spatiotemporal variation and sensitivity of the temperature (i.e. TR and TS) for rain to snow transition. For example, based on the United States Army Corps of Engineers (1956) study, Sproles *et al.* (2013) approximated the precipitation phase transition between TS $= -2$ and TR $= +2$ °C in the McKenzie River Basin of Oregon Cascades. Klos *et al.* (2014) used TS $= -2$ and TR $= +4$ °C, based on the findings of Dai (2008), for partitioning total precipitation into snow and rain across the western United States. For the purpose of this study, we performed a sensitivity analysis on S_f by varying the TS between -2.0 and 0 °C and TR between -1.0 and 4.0 °C in 0.5 °C increments. The values of S_f were calculated for all possible pairs ($n = 49$) of TS and TR with condition of TS $<$ TR. Among the four regions, S_f sensitivity (expressed in terms of standard deviation) to TS and TR varied spatially within a specific region with highest sensitivity centered (with the exception of GB) around 50% S_f (Figure 2). In GB, the distribution of S_f sensitivity was slightly skewed toward higher values of S_f. This suggested that choice of TS and TR is particularly critical for characterizing the S_f variability in this region. To identify the representative TS and TR value for our study domain, we correlated the winter season positive changes (i.e. snow accumulation) in SWE and empirically calculated SFE using Equation (1) at 733 Snow Telemetry (SNOTEL) sites (available via: http://www.wcc.nrcs.usda.gov/snow/). The average length of the concurrent SWE, precipitation, and temperature record during 1980–2012 was 25 years. Note that in this case not all positive changes in SWE were related to snowfall. In the transitional snow zone, rain-on-snow could also result in positive SWE. Using TS $= -2$ °C and TR $= +2$ °C, we found strong agreement between observed SWE (mm) and calculated SFE (mm), with 78% of the total SNOTEL sites had an $R^2 > 0.5$ and 40% of the sites had an $R^2 > 0.8$ (Figure 1(b)). In terms of percent bias (PBIAS), 25% of the total SNOTEL sites had a PBIAS within 10% of observed SWE and 77% had a PBIAS within 25% of the observed SWE (Figure 1(c)). The absolute biases of 69% of the sites were less than 5 cm and 89% of the sites were less than 10 cm. Also, the PBIAS between observed SWE and calculated SFE was consistent among wet (average PBIAS $= -13.7\%$) and dry (average PBIAS $= -14.9\%$) winters. On average the agreement between observed SWE and calculated SFE was slightly better during cold (average PBIAS $= -3.9\%$) than those during warm (average PBIAS $= -22.4\%$) winters. Irrespective of climate extremes (i.e. wet, dry, cold, and warm), at the majority of the sites PBIAS was negative, indicating that TS $= -2$ °C and TR $= +2$ °C resulted

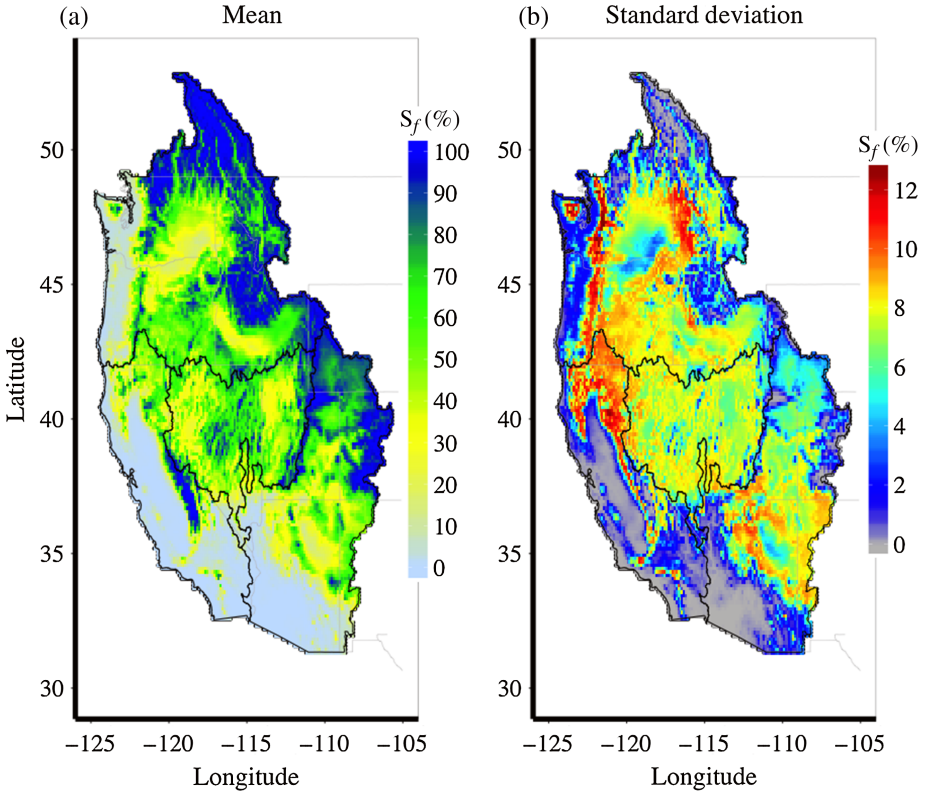

Figure 2. Spatial variability in (a) mean and (b) standard deviation of snow fraction (S_f) estimated using varying temperature thresholds (i.e. TR and TS) for rain to snow transition.

in lower SWE values than those observed at the SNOTEL sites. However, most of the sites with large negative PBIAS were located at lower elevations where using positive changes in SWE to validate SFE would have been problematic. At these lower elevation sites, as mentioned above, rain-on-snow events may result in an increase in SWE. In addition, because of warmer temperatures at these lower elevation sites, snowfall and melt may occur simultaneously with no net increase in daily SWE. By increasing TR, this negative PBIAS was reduced, but resulted in more sites with positive PBIAS. This suggested that the value of TS and TR are site specific, but the lack of spatially distributed SWE measurements limited our ability to derive such parameters across the study domain. However, we plan to investigate the variability in TS and TR at the SNOTEL sites in the subsequent work. For the purpose of this study, we approximated the precipitation phase transition as between TS = −2 and TR = +2 °C. We considered the choice of TS and TR values as a potential source of uncertainty in the estimated S_f and discuss the implications below.

2.3. Retrospective snow fraction sensitivity and trend analysis

Spatially averaged November–March total P was used to define the 10 wettest and driest winters during 1916–2003 for each of the four regions by ranking the November–March total P time series. Similarly, 10 coldest and warmest winters were defined after ranking the spatially average T_{w_avg} for each of the four regions. To capture the natural variability of climatic extremes during the study period we used 10 as opposed to 5 years of data to define the extremes (e.g. Mishra and Cherkauer, 2011). We used a Mann–Whitney–Wilcoxon rank sum test ($p = 0.05$) to test differences in S_f between cold and warm, and between wet and dry winters, across all the four regions. Mean S_f for the 10 coldest (cold) and warmest (warm) winters and corresponding T_{w_avg} were used to define the temperature sensitivity of S_f as:

$$\varepsilon_T = \frac{S_f\,(\text{cold}) - S_f\,(\text{warm})}{T_{w\_avg}\,(\text{cold}) - T_{w\_avg}\,(\text{warm})} \tag{3}$$

Similarly, precipitation sensitivity of S_f can be calculated as:

$$\varepsilon_P = \frac{S_f\,(\text{wet}) - S_f\,(\text{dry})}{P\,(\text{wet}) - P\,(\text{dry})} \tag{4}$$

The Theil–Sen approach (Sen, 1968) and non-parametric Kendall's tau tests (Kendall, 1938) were used to identify trends in the annual S_f time series. Monotonic trends were classified as 'detectable' when their signal-to-noise ratios (SNR) were >1. The SNR was defined as the absolute change in S_f calculated from the monotonic trend divided by the standard deviation over a given period of interest (Déry *et al.*, 2011). To evaluate spatial and temporal consistency in the S_f changes, both trend and SNR analysis were performed for long-term (1916–2003) and most recent (1960–2003) time periods. Observed trends in hydro-climatological data can be

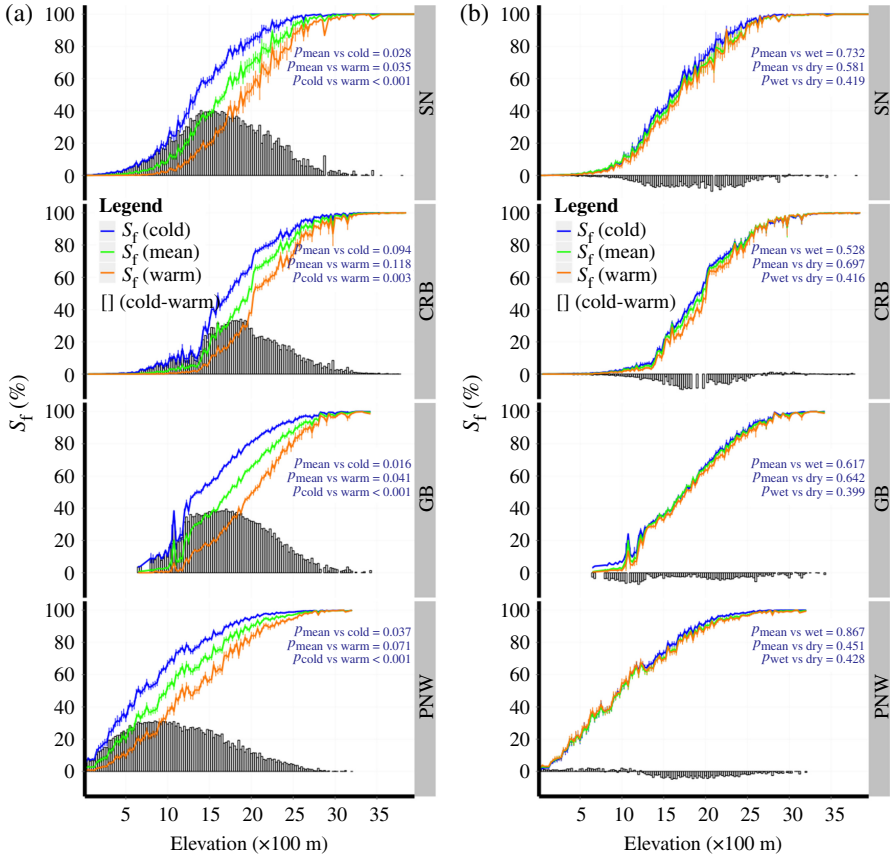

Figure 3. Elevation dependence of average snow fraction across the four study regions during 1916–2003 climatological mean (mean) and (a) the 10 coldest winters (cold), 10 warmest winters (warm), and the difference between them (grayscale bars), (b) the 10 wettest winters (wet), 10 driest winters (dry), and the difference between them (grayscale bars). Error bars associated with line plot show the standard error of mean S_f for each 100-m elevation bin.

highly sensitive to the time period over which trends are evaluated; especially when length of record is short and start/end years fall during episodes of strong large-scale climate variability (i.e. the Pacific Decadal Oscillation and El Niño Southern Oscillation). For this reason we choose 1960, an El Niño Southern Oscillation neutral year, as a starting point for our short-term trend evaluation.

2.4. Snow fraction under projected climate

Potential effects of a warmer climate on S_f were simulated using the average changes in the PNW temperature from 20 climate models and two greenhouse gas emissions scenarios (B1 and A1B) for the 2020s, 2040s, and 2080s (Mote and Salathé, 2009). The projected changes in temperature under the A1B scenario for CRB, GB, and SN were kept the same as those predicted for the PNW. These warming scenarios were generated after modifying the daily air temperature using the delta method (Hay *et al.*, 2000) and keeping daily precipitation constant. The daily temperature values were increased uniformly by 1.1, 1.8, and 3.0 °C for 2020, 2040, and 2080 warming scenarios, respectively. In this study, effects of future changes in precipitation on S_f were not considered, since both magnitude and direction of future precipitation, as predicted by global circulation models, are highly uncertain for this region. Although recent trend analysis in historical precipitation showed an increase in spring precipitation and decrease in summer and autumn precipitation (Abatzoglou *et al.*, 2014), there is no agreement in future precipitation projections from global circulation models. Mote and Salathé (2009) reported a small increase (1–2%) in the annual precipitation of the Pacific Northwest region of the study domain under B1 and A1B emission scenarios from the Intergovernmental Panel on Climate Change (IPCC) Fourth Assessment Report (AR4). In contrast, Ficklin *et al.* (2014) reported an average increase of 14.4% in annual precipitation of the Columbia River Basin under radiative forcing of 8.5 w/m^2 (RCP 8.5) of the Coupled Model Inter-comparison Project – phase 5 (CMIP5). This higher increase in precipitation could have been an artifact of the differences in the emission scenarios between AR4 and CMIP5 and positive CMIP5 model bias (Mehran *et al.*, 2014).

3. Results

3.1. Snow fraction variability

To investigate the variability in S_f under different climate extremes, we examined S_f as a function of elevation during the coldest and warmest (Figure 3(a)) and wettest and driest winters (Figure 3(b)). For mean and extreme (dry,

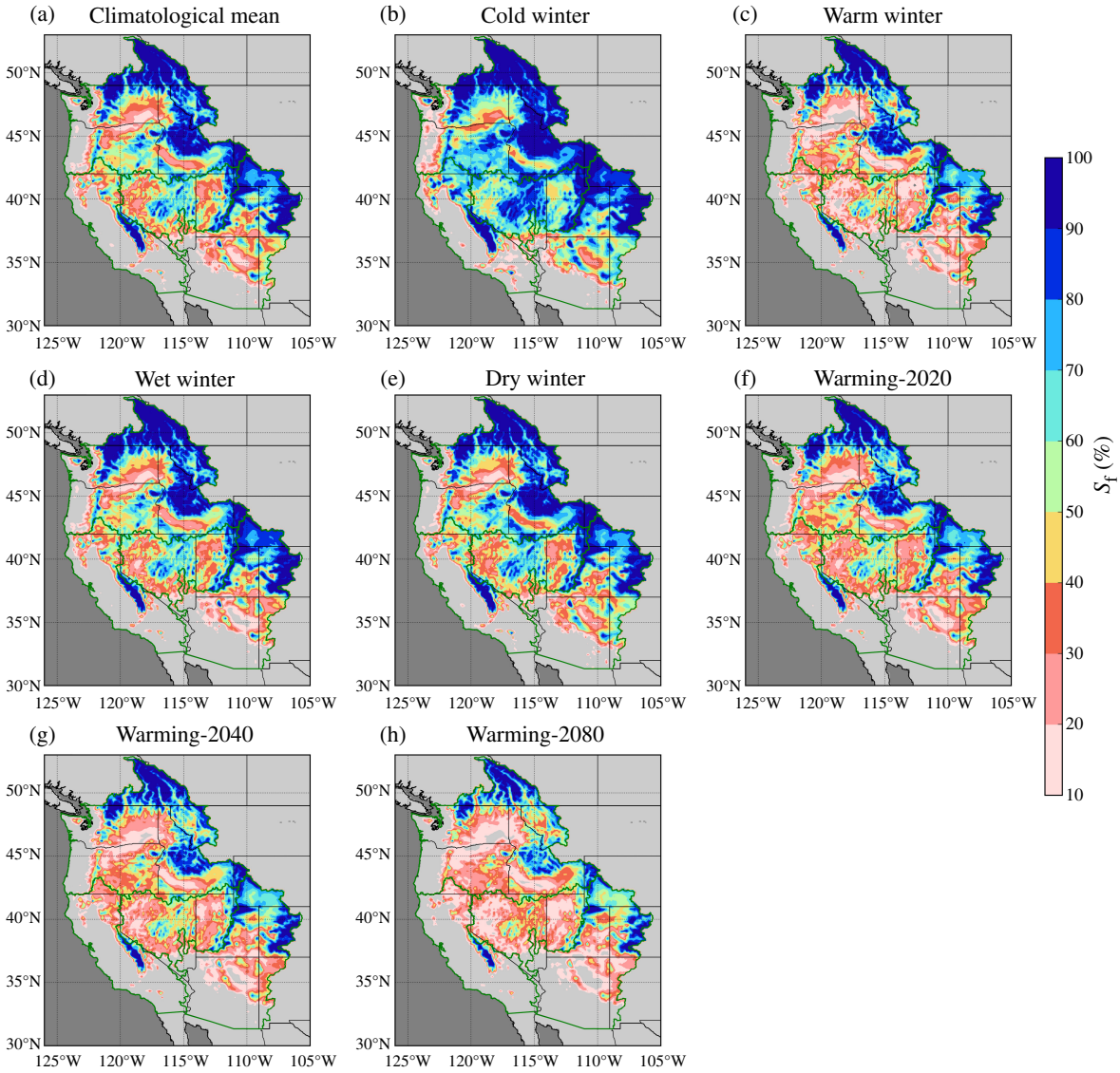

Figure 4. Average snow fraction (S_f %) during (a) climatological mean 1916–2003, (b) 10 coldest winters, (c) 10 warmest winters, (d) 10 wettest winters, (e) 10 driest winters, (f) 2020 warming scenario, (g) 2040 warming scenario, and (h) 2080 warming scenario.

wet, cold or warm) winters, S_f showed a logistic relationship with elevation across all four regions. As expected, there were contrasting differences in S_f at similar elevations between the four regions. PNW showed significantly higher S_f at lower elevations when compared with SN, CRB, and GB, which can be attributed to latitudinal differences. S_f reached 100% at elevations just above 2000 m in PNW as compared with nearly 2500 m in SN, CRB, and GB (Figure 3). The highest S_f regions were along the Cascade and Rocky Mountains in PNW, the southern part of SN, and the Wasatch Range in CRB and GB during climatological mean (Figure 4(a)), cold (Figure 4(b)) and warm (Figure 4(c)), as well as during wet (Figure 4(d)) and dry winters (Figure 4(e)). The S_f in northern Cascades, northern Rockies, southern SN, and Wasatch Range remains elevated during all climate extremes.

A two sample non-parametric Mann–Whitney–Wilcoxon rank sum test showed statistically significant differences ($p < 0.05$) between cold and warm winter S_f across all four regions. In PNW, the difference in S_f between the historical mean and those during warm winters was not statistically significant ($p > 0.05$). This indicated that in PNW the S_f distribution was skewed toward warm winters. In CRB, there were no statistically significant differences in mean S_f and those during extreme cold and warm winters. However, the difference in S_f during warm and cold winters was statistically significant ($p < 0.05$). The difference in S_f between cold and warm winters was large at mid-elevations (Figure 3(a)). Geographically, there were large differences in cold (Figure 4(b)) and warm (Figure 4(c)) winter S_f in the northern part of SN, central part of CRB, both eastern and western edges of GB, and the Columbia Plateau, Snake River Plain and much of the eastern Oregon in PNW. The greatest change in S_f between cold and warm winters across elevation (shown as the bar chart in Figure 3) occurred in SN (40%) followed by GB (39%), CRB (34%), and PNW (31%). These findings were inconsistent

Table 1. Variability of winter season (November–March) precipitation (P) and average wet day temperature (T_{w_avg}) and their influence on snowfall to precipitation ratio (S_f) for the 10 coldest and 10 warmest years, selected based on domain-averaged P and T_{w_avg} for the period 1916–2003 in the Sierra Nevada (SN), Colorado River Basin (CRB), Great Basin (GB), and Pacific Northwest (PNW).

	SN			CRB				GB				PNW			
Year	P (mm)	T_{w_avg} (°C)	S_f (%)	Year	P (mm)	T_{w_avg} (°C)	S_f (%)	Year	P (mm)	T_{w_avg} (°C)	S_f (%)	Year	P (mm)	T_{w_avg} (°C)	S_f
Cold															
1917	390	2.7	28.9	1917	128	−2.5	63.3	1917	140	−4.1	78.9	1916	644	−4.4	70.4
1922	452	4.0	25.2	1930	116	−0.6	49.8	1923	138	−2.7	73.0	1917	476	−5.3	76.4
1923	336	3.8	26.8	1932	176	−0.7	50.4	1930	118	−2.9	59.9	1922	502	−4.6	68.8
1932	402	3.2	27.9	1933	106	−3.0	59.7	1932	152	−3.9	71.5	1923	472	−4.4	70.6
1933	349	2.2	33.7	1937	177	−0.9	49.8	1933	118	−5.7	77.2	1929	375	−4.2	65.8
1937	442	3.0	30.2	1949	162	−1.8	54.4	1937	172	−4.6	71.4	1937	435	−5.5	72.8
1949	391	2.5	31.5	1952	197	−0.3	48.6	1944	145	−2.5	63.8	1949	532	−5.1	68.7
1950	433	4.1	23.6	1955	117	−0.5	49.5	1949	165	−5.3	72.3	1952	520	−4.2	70.0
1952	611	3.4	25.7	1974	129	−0.3	48.3	1952	215	−3.0	67.6	1969	574	−4.5	68.2
1969	644	4.1	23.6	1979	265	−0.4	43.1	1955	148	−3.1	57.8	1979	444	−4.5	65.8
Mean	*445*	*3.3*	*27.7*	–	*157*	*−1.1*	*51.7*	–	*151*	*−3.8*	*69.3*	–	*497*	*−4.7*	*69.8*
Warm															
1934	316	6.5	12.8	1934	96	3.1	30.9	1934	113	1.4	35.1	1934	573	−0.1	45.2
1940	548	6.9	10.8	1938	168	2.5	32.7	1961	132	0.8	38.7	1940	540	−0.7	47.3
1963	364	7.0	11.0	1961	113	2.5	38.9	1963	127	0.4	36.7	1958	527	−1.0	53.6
1970	518	6.8	11.4	1978	218	2.4	34.0	1970	158	0.6	36.6	1961	592	−0.7	50.4
1978	591	6.6	14.4	1981	134	3.2	31.4	1978	188	0.9	37.5	1963	479	−1.1	48.4
1980	536	6.6	13.4	1986	161	2.4	35.4	1981	158	1.2	35.2	1981	517	−0.1	44.0
1981	400	6.5	13.4	1995	206	2.8	32.8	1986	195	0.4	41.6	1983	631	−0.6	50.6
1992	350	6.6	15.3	1996	128	2.5	31.9	1992	132	1.3	38.3	1992	436	−0.2	46.9
2000	450	6.4	15.1	2000	115	2.6	36.9	2000	150	0.4	43.9	2000	578	−1.2	56.0
2003	489	7.4	8.9	2003	148	2.7	31.0	2003	126	1.1	28.5	2003	563	0.4	42.9
Mean	*456*	*6.7*	*12.7*	–	*149*	*2.7*	*33.6*	–	*148*	*0.9*	*37.2*	–	*544*	*−0.5*	*48.5*
Cold–Warm	**−11**	**−3.4**	**15.0**	–	**8**	**−3.8**	**18.1**	–	**3**	**−4.7**	**32.1**	–	**−47**	**−4.2**	**21.3**

Gray shading indicates wettest and driest year for each region.

Table 2. Variability of winter season (November–March) precipitation (P) and average wet day temperature (T_{w_avg}) and their influence on snowfall to precipitation ratio (S_f) for the 10 wettest and 10 driest years, selected based on domain-averaged P and T_{w_avg} for the period 1916–2003 in the Sierra Nevada (SN), Colorado River Basin (CRB), Great Basin (GB) and Pacific Northwest (PNW).

	SN			CRB				GB				PNW			
Year	P (mm)	T_{w_avg} (°C)	S_f (%)	Year	P (mm)	T_{w_avg} (°C)	S_f (%)	Year	P (mm)	T_{w_avg} (°C)	S_f (%)	Year	P (mm)	T_{w_avg} (°C)	S_f
Wet															
1938	649	5.6	16.5	1916	219	0.8	45.1	1916	194	−2.4	61.4	1916	644	−4.4	70.4
1952	611	3.4	25.7	1920	203	1.2	44.7	1952	215	−3.0	67.6	1938	638	−1.9	57.6
1956	603	4.6	19.0	1941	210	1.9	38.3	1969	197	−1.9	60.3	1956	696	−4.0	66.6
1969	644	4.1	23.6	1952	197	−0.3	48.6	1980	204	0.4	38.6	1971	660	−2.7	58.6
1978	591	6.6	14.4	1978	218	2.4	34.0	1982	213	−0.4	50.8	1972	684	−3.0	61.4
1982	611	5.8	16.6	1979	265	−0.4	43.1	1983	216	0.3	42.7	1974	775	−1.7	53.7
1983	744	5.7	15.6	1980	233	2.2	36.3	1984	216	−1.2	57.2	1982	677	−2.3	55.1
1986	586	6.2	13.8	1983	218	2.0	36.1	1986	195	0.4	41.6	1996	690	−1.5	53.6
1995	681	5.5	16.5	1993	256	1.0	37.1	1995	200	−0.1	43.6	1997	760	−2.4	61.0
1998	670	5.8	16.8	1995	206	2.8	32.8	1997	192	−0.5	46.3	1999	746	−1.4	56.7
Mean	*639*	*5.3*	*17.9*	–	*223*	*1.4*	*39.6*	–	*204*	*−0.8*	*51.0*	–	*697*	*−2.5*	*59.5*
Dry															
1920	302	4.6	23.5	1933	106	−3.0	59.7	1924	116	−2.0	58.4	1924	418	−2.6	61.1
1924	242	4.9	20.0	1934	96	3.1	30.9	1926	126	−0.6	46.1	1926	408	−1.4	57.5
1929	304	4.3	22.6	1946	106	0.4	44.7	1930	118	−2.9	59.9	1929	375	−4.2	65.8
1931	276	6.2	17.0	1959	102	1.4	42.8	1931	100	−1.6	60.2	1930	426	−3.6	62.9
1934	316	6.5	12.8	1964	108	0.5	47.7	1933	118	−5.7	77.2	1931	396	−2.1	58.9
1948	314	4.6	20.6	1972	93	0.0	44.7	1934	113	1.4	35.1	1941	389	−1.2	55.3
1976	249	4.6	21.7	1977	96	0.3	45.5	1977	93	−1.5	53.2	1944	331	−2.4	60.3
1977	210	4.8	20.7	1990	104	1.1	43.7	1987	123	−0.2	46.3	1977	291	−2.0	60.4
1990	256	4.3	22.0	1999	101	2.2	35.8	1990	107	−1.4	52.5	1994	404	−1.8	60.7
2001	322	4.9	21.5	2002	74	1.4	43.3	1991	119	−1.1	47.7	2001	297	−2.8	65.1
Mean	*279*	*5.0*	*20.2*	–	*99*	*0.7*	*43.9*	–	*113*	*−1.6*	*53.7*	–	*374*	*−2.4*	*60.8*
Wet–Dry	**360**	**0.3**	**−2.3**	–	**124**	**0.7**	**−4.3**	–	**91**	**0.8**	**−2.7**	–	**324**	**−0.1**	**−1.3**

Gray shading indicates wettest and driest year for each region.

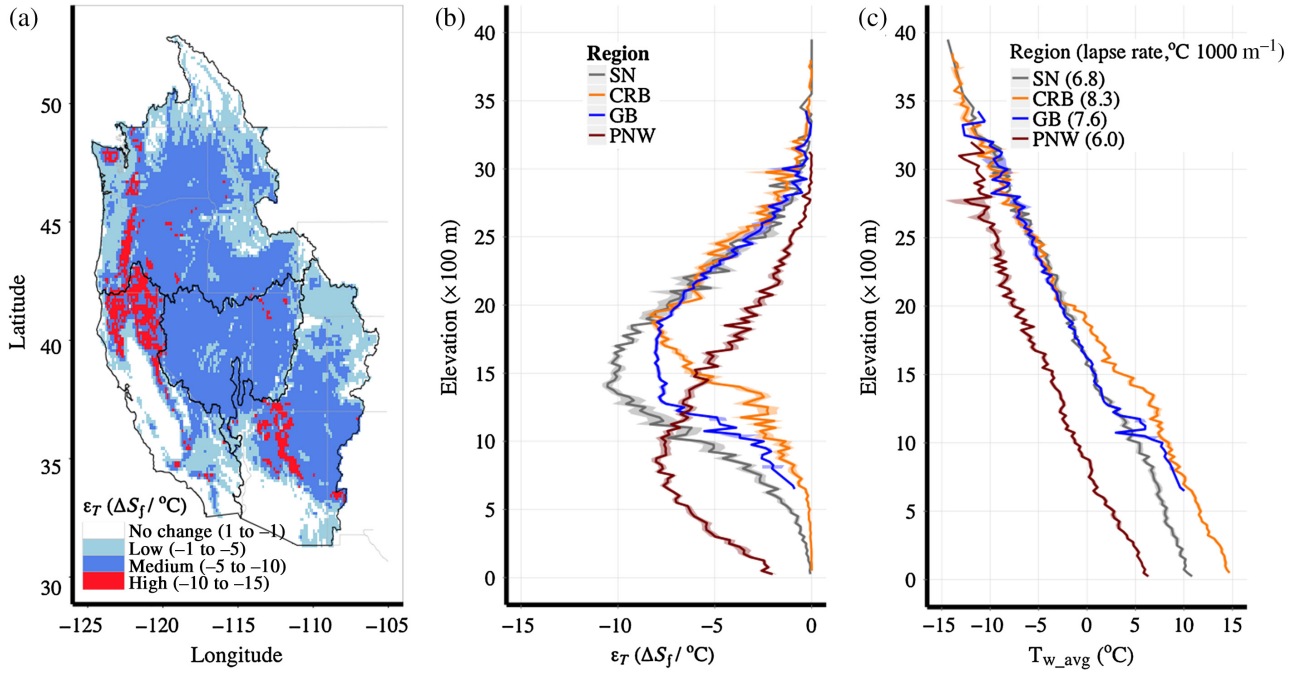

Figure 5. (a) Spatial distribution of temperature sensitivity of snow fraction (ε_T), (b) elevation dependence of ε_T, and (c) elevation dependence of T_{w_avg}. The ε_T and T_{w_avg} values were binned in 100-m elevation intervals and are shown as the mean (solid lines) and standard error (shading) for each bin.

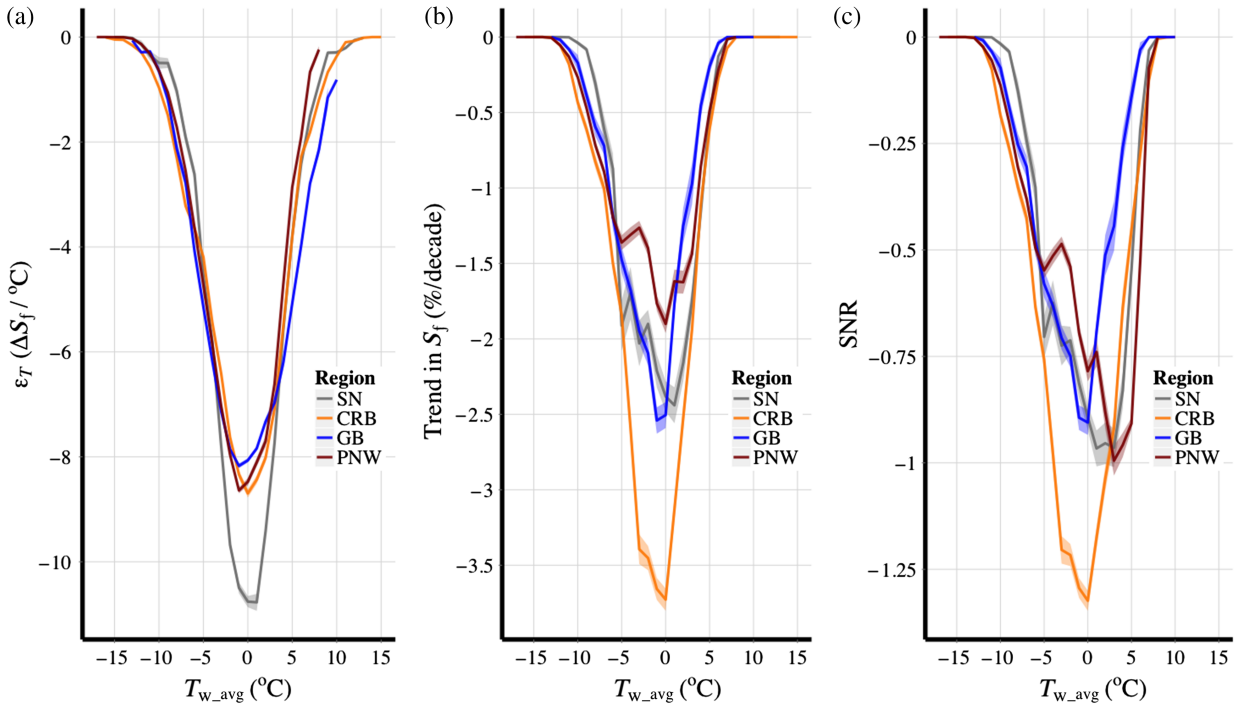

Figure 6. Temperature dependence (T_{w_avg}) of (a) temperature sensitivity of snow fraction (ε_T), (b) trends in snow fraction (S_f) and (c) signal-to-noise ratio (SNR) across regions. The ε_T, S_f, and SNR values were binned in 1 °C T_{w_avg} intervals and are shown as the mean (solid lines) and standard error (shading) for each bin.

with the corresponding change in T_{w_avg} between cold and warm winters (Table 1). Although the average change in temperature across all elevation grids between cold and warm winters was smallest (−3.4 °C) in SN and largest (−4.7 °C) in GB, both showed a similar change in S_f. This was attributed to overall warmer temperatures in SN, where a small change in temperature led to a larger change in S_f. In contrast, the change in S_f in PNW between cold and warm winters was the smallest despite a larger (−4.2 °C) change in temperature, because of overall colder temperatures during both cold and warm winters (Table 1). Winter season precipitation during cold and

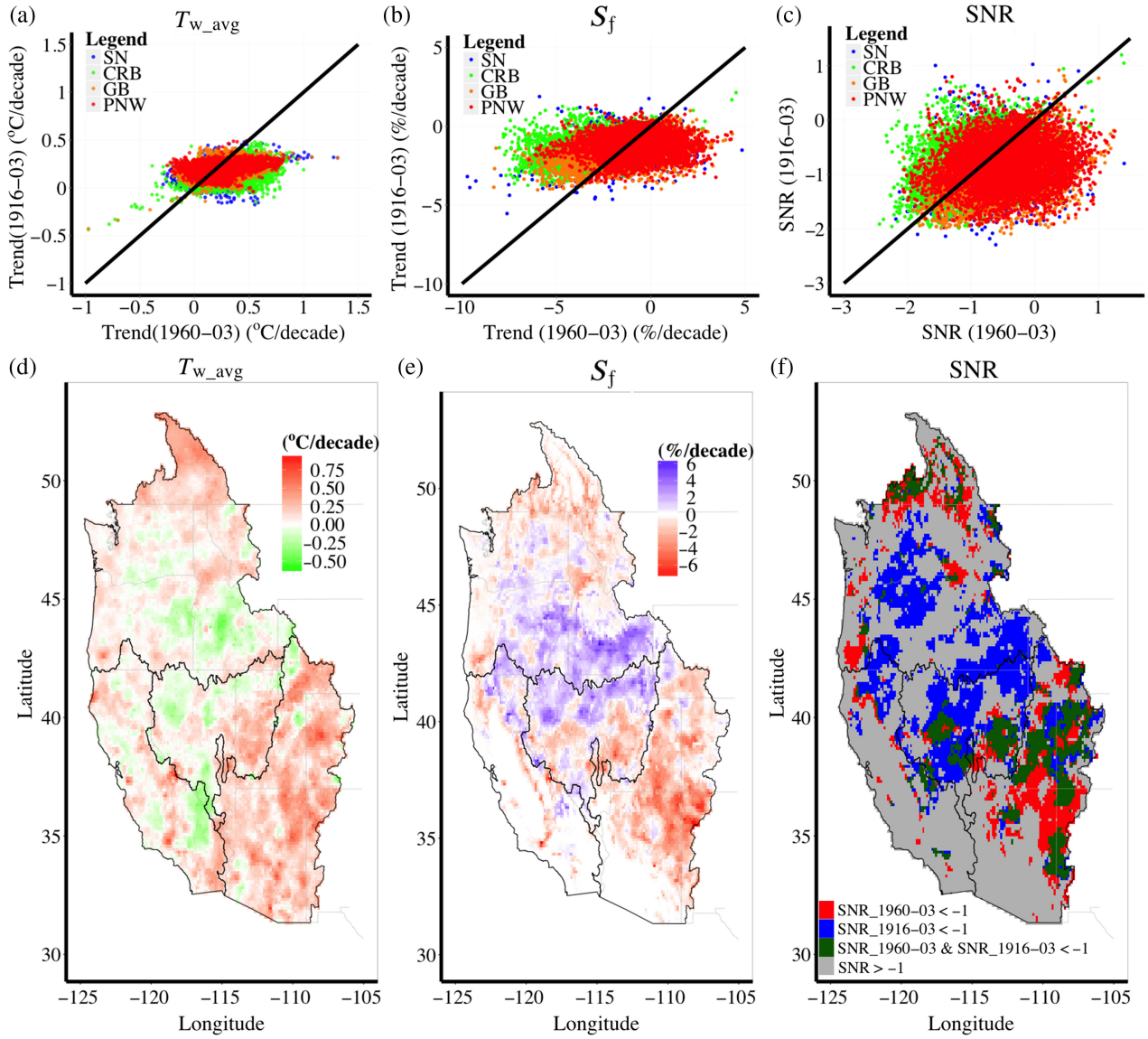

Figure 7. Comparison of long-term (1916–2003) and recent (1960–2003) trends with 1 : 1 line (solid black) in (a) average winter wet day temperature (T_{w_avg}), (b) snow fraction (S_f), and (c) corresponding signal-to noise ratios (SNR) in S_f. Spatial trends (d and e) and spatial shifts (f) are reported as the difference between values for recent and long-term periods.

warm years was similar across the four regions (Table 1). During warm winters, precipitation was higher by as much as 10% in PNW and lower by as much as 5% in CRB as compared with precipitation during cold winters. Across all four regions the majority of cold winters occurred prior to 1950 and the majority of warm winters occurred after 1970 (Table 1).

A nearly twofold increase in precipitation during extreme wet years (Table 2) showed no influence on S_f across all the four regions (Figure 4(d) and (e)). In fact, S_f during dry winters was marginally higher (Figure 3(b)) compared with wet winters, particularly in SN and CRB, which can be attributed to relatively cold temperatures in those regions (Table 2), although this was not statistically significant ($p > 0.05$). Similar to cold and warm winters, the majority of the 10 driest and wettest winters during the period 1916–2003 were prior to and post 1950, respectively, except in CRB where both extremes occurred predominantly after 1950s (Table 2). Year 1977, one of the driest on record, ranked higher in terms of S_f because of colder temperatures. In general, S_f was lower when a dry or wet year was associated with warm temperatures (e.g. 1934 in SN, CRB, GB, and 1941 in PNW), suggesting that temperature trumped precipitation in determining S_f.

3.2. Retrospective snow fraction sensitivity and trends

The temperature sensitivity of S_f (ε_T) varied significantly among regions (Figure 5). The S_f along the Cascade and Olympic mountain ranges in PNW, Klamath and northern Sierra in SN, and part of the lower CRB was most sensitive to temperature (Figure 5(a)). An increase in temperature by 1 °C could result in a decrease of 10–15% S_f in these regions. In terms of elevation, the medium and high sensitivity ($\varepsilon_T < -5$) regions were between 1000–2200 m in SN, 1500–2000 m in CRB, 1200–2200 m in GB, and

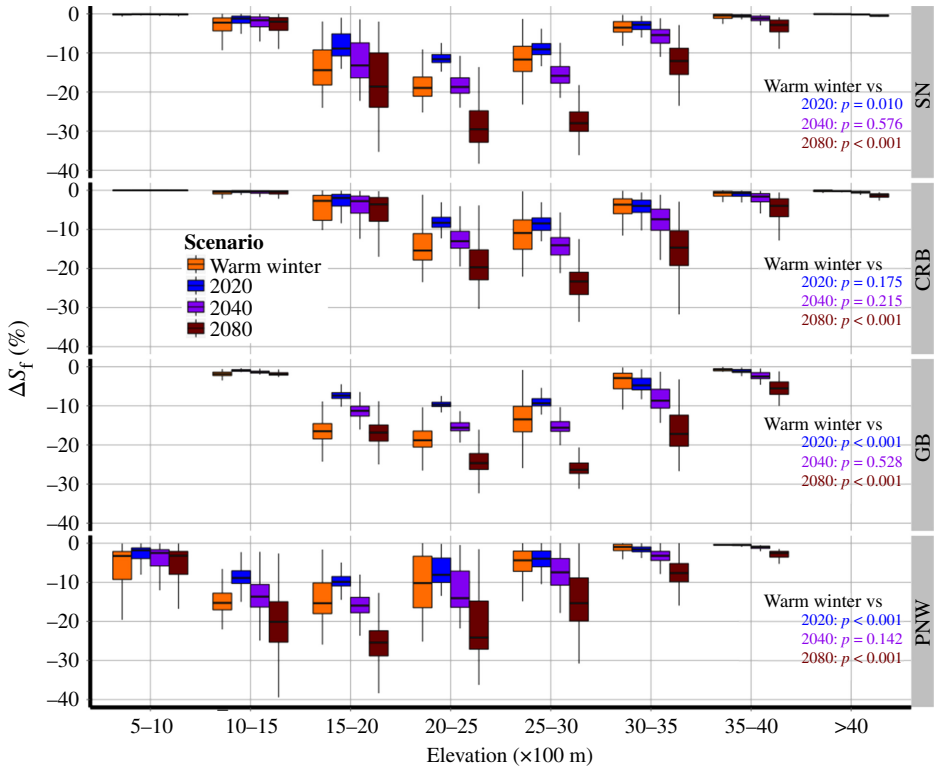

Figure 8. Decline in S_f with respect to climatological mean under historical warm winter, 2020, 2040, and 2080 scenarios. The line inside the box represents the median value, the box itself represents the interquartile range (IQR) (25th–75th percentile range) and the whiskers are the lowest and highest values within 1.5 × IQR of the 25th and 75th percentiles.

300–1500 m in PNW (Figure 5(b)). These highly sensitive S_f regions were very similar to 'at-risk' snow mapping developed by Nolin and Daly (2006) for the Pacific Northwest. The pattern in *elevation*–ε relationship (Figure 5(b)) can be characterized by the *elevation*-T_{w_avg} profile or lapse rate among the four regions (Figure 5(c)).

Most of the medium and high ε_T regions had T_{w_avg} between −5 and 5 °C (Figure 6(a)) and followed monotonic trends (Figure 6(b)) and SNR (Figure 5(c)) in S_f very closely. However, despite higher S_f sensitivity between −5 and 5 °C temperature range in SN, the monotonic trend and SNR in SN were comparable with those in PNW and GB. In contrast, ε_T between −5 and 5 °C temperature range in CRB was similar to those in PNW and GB, but showed much higher monotonic trend than SNR. These contrasting patterns indicated that in CRB the monotonic trend in S_f supersedes the historic variability in S_f, whereas, in SN historical variability in S_f supersedes the monotonic trend. Because there was no statistically significant difference in S_f between wet and dry years, precipitation sensitivity of S_f, ε_P, was excluded from further analysis.

Comparative analyses of long-term (1916–2003) and recent (1960–2003) monotonic trends indicated an increase in warming indicated by T_{w_avg} during the most recent time period (Figure 7(a)). Since 1960, T_{w_avg} has increased on average by 1.4 (SN), 2.5 (CRB), 1.3 (GB), and 1.3 (PNW) times faster as compared with the long-term trend. In terms of absolute magnitude, the recent rate of warming in T_{w_avg} has been higher by as much as 1.0 °C decade^{-1} (Figure 7(d)). The effect of this recent rapid warming in T_{w_avg} was clearly reflected in S_f trends. An overall downward trend in S_f was observed during both long-term and recent periods (Figure 7(b)). The long-term (1916–2003) downward trend in S_f was statistically significant for 37, 45, 76, and 63% of the grid cells in SN, CRB, GB, and PNW, respectively. Regionally, the average significant decreasing trend ranged from 1.3% decade^{-1} in SN to 1.9% decade^{-1} in GB. The spatial extent of the statistically significant trend during the recent period (1960–2003) was reduced to 12, 42, 19, and 23% of the grid cells in SN, CRB, GB, and PNW, respectively. However, the regional average significant decreasing trend ranged from 1.6% decade^{-1} in PNW to 3.9% decade^{-1} in GB, showing a more rapid decline during the recent period. This large decline in S_f during 1960–2003 as compared to 1916–2003 was 2.1 and 2.3 times higher in CRB and GB, respectively (Figure 7(e)).

Similar to the trend analyses, the SNR analyses showed a greater reduction in S_f during the period 1960–2003 as compared with the period 1916–2003 (Figure 7(c)). Trends in 16, 27, 54, and 31% of the grid cells in SN, CRB, GB, and PNW, respectively were detectable ($|SNR| > 1$) during the period 1916–2003. During the more recent period 1960–2003, the spatial extent of detectable trend decreased to 7, 21, and 16% of the grid cells in SN, GB, and PNW, respectively, but increased to 40% of the grid cells in CRB. This indicates that not only did a greater percentage of CRB grid cells show a decreasing trend in S_f during the recent period but also that the magnitude of the trend was exceeded by the natural annual variability. Also, in the

Table 3. Watershed average snow fraction (S_f) under historical climate (climatological mean), 10 warmest winters (warm winter), and three future warming scenarios (i.e. 2020, 2040, and 2080).

HUC4 watershed	Watershed average S_f (%)				
	Climatological mean	Warm winter	2020	2040	2080
Bear	79 (5)	69 (7)	72 (6)	67 (6)	59 (7)
Black Rock Desert-Humboldt	56 (8)	38 (8)	46 (7)	41 (7)	32 (6)
Central Lahontan	50 (7)	33 (7)	41 (7)	36 (6)	28 (6)
Central Nevada Desert Basins	52 (7)	35 (8)	43 (7)	38 (6)	30 (6)
Colorado Headwaters	87 (3)	83 (4)	82 (4)	79 (4)	72 (5)
Escalante Desert-Sevier Lake	61 (7)	47 (8)	52 (7)	47 (7)	38 (6)
Great Divide-Upper Green	87 (4)	83 (5)	81 (5)	77 (5)	70 (6)
Great Salt Lake	54 (7)	39 (8)	46 (7)	40 (6)	32 (6)
Gunnison	88 (3)	83 (4)	83 (4)	80 (4)	74 (5)
Klamath-Northern California Coastal	30 (7)	19 (6)	23 (6)	19 (5)	13 (4)
Kootenai-Pend Oreille-Spokane	79 (6)	72 (6)	72 (6)	66 (7)	57 (7)
Little Colorado	42 (7)	30 (7)	33 (7)	28 (6)	21 (5)
Lower Colorado-Lake Mead	31 (6)	19 (6)	24 (5)	20 (5)	14 (4)
Lower Columbia	27 (6)	18 (5)	20 (5)	16 (5)	11 (3)
Lower Green	73 (5)	65 (6)	67 (5)	62 (5)	55 (6)
Lower Snake	70 (5)	62 (6)	63 (6)	58 (6)	49 (6)
Middle Columbia	44 (7)	32 (7)	35 (7)	30 (6)	23 (5)
Middle Snake	63 (7)	48 (8)	54 (7)	48 (7)	39 (7)
North Lahontan	51 (9)	31 (9)	40 (8)	34 (8)	25 (6)
Northern Mojave-Mono Lake	23 (4)	15 (3)	19 (3)	16 (3)	13 (2)
Oregon Closed Basins	58 (8)	40 (9)	48 (8)	42 (8)	32 (7)
Oregon-Washington Coastal	14 (4)	8 (3)	10 (3)	8 (2)	5 (2)
Puget Sound	32 (5)	26 (5)	26 (5)	23 (4)	17 (4)
Sacramento	27 (6)	18 (5)	21 (5)	17 (4)	12 (4)
Salt	24 (6)	15 (5)	18 (5)	15 (4)	10 (3)
San Joaquin	25 (2)	22 (2)	23 (2)	21 (2)	18 (2)
San Juan	54 (7)	43 (8)	45 (7)	40 (7)	31 (6)
Tulare-Buena Vista Lakes	22 (2)	18 (2)	19 (2)	18 (2)	15 (2)
Upper Colorado-Dirty Devil	55 (7)	44 (7)	47 (6)	42 (6)	34 (6)
Upper Colorado-Dolores	64 (6)	54 (7)	56 (6)	52 (6)	43 (6)
Upper Columbia	72 (5)	64 (6)	65 (6)	60 (6)	52 (6)
Upper Gila	20 (5)	15 (4)	15 (4)	12 (3)	8 (3)
Upper Snake	74 (5)	63 (7)	67 (6)	63 (6)	55 (6)
White-Yampa	80 (5)	74 (6)	73 (5)	69 (6)	61 (6)
Willamette	23 (5)	15 (5)	17 (5)	14 (4)	9 (3)
Yakima	59 (7)	48 (8)	49 (8)	44 (8)	34 (7)

Parenthetical values are one standard deviation and express variability in the estimates due to the plausible range of TR (−1 to +4 °C) and TS (−2 to 0 °C) threshold values ($n = 49$).

majority of the grid cells the detectable decreasing trends (SNR < -1) during 1916–2003 and 1960–2003 did not overlap, indicating a geographical shift towards a decline in S_f during recent time (Figure 7(f)).

3.3. Effects of climate warming on snow fraction

The projected S_f for 2020 (Figure 4(f)), 2040 (Figure 4(g)), and 2080 (Figure 4(h)) warming scenarios showed a significant decline, particularly along the Cascade and Olympic mountains in the PNW region. However, higher elevations in southern SN, northern Rockies, and Wasatch Range (Figure 1(a)) would continue to be dominated by higher S_f. Much of the southern Cascade and Olympic Mountains in PNW and GB would experience more rain than snow under the 2080 warming scenario. On average, the decrease in S_f under warm winters and future warming scenarios in the SN, CRB, GB, and PNW regions ranged from 7 to 16%, 4 to 9%, 6 to 14%, and 10 to 22%, respectively. The declines in S_f under warm winters place results from future warming scenarios in the context of historical climate variability. GB and SN showed the largest and smallest changes, respectively, under all four scenarios. However, at mid-elevations, PNW and SN showed the greatest decrease in S_f, followed by GB and CRB (Figure 8). The difference in S_f between the historical average and warmest winters most closely resembles the 2040 warming scenario in all the four regions except GB. In GB, the difference in S_f under warm winters is higher at lower elevations and lower at higher elevations compared with the 2040 warming scenario. An increase of temperature by 3 °C under the 2080 warming scenario resulted in S_f even lower than current extreme warm winters across all the four regions. As expected, the warming showed greater impact on S_f at mid-elevations. However, the zone of influenced elevation expands with increasing temperature.

The comparison of average S_f at the USGS Hydrologic Unit Code sub-regional scale (HUC4) under historical

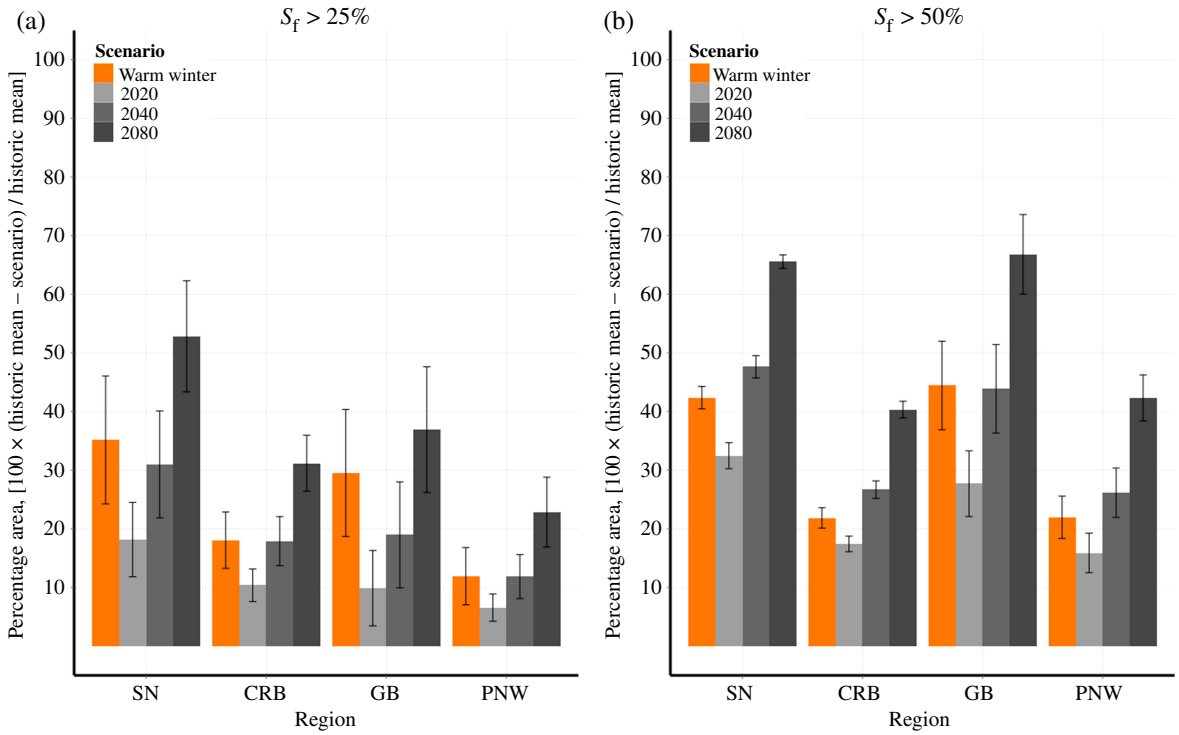

Figure 9. Average decline in snowfall dominated (a) $S_f > 25\%$ and (b) $S_f > 50\%$ area under warm winter conditions (showing historical range) and under three warming (2020, 2040, and 2080) scenarios. The error bars show ± one standard deviation across the plausible range of TR (−1 to +4 °C) and TS (−2 to 0 °C) threshold values ($n = 49$).

climate, warm winter, and three future warming scenarios showed significant declines across all the watersheds (Table 3). The uncertainty in S_f estimates (expressed in terms of standard deviation) associated with the choice of TR and TS was far smaller than projected changes in S_f. By 2020, 8% of the watersheds showed S_f lower than the average S_f during the 10 warmest winters, which increased to 58% by 2040 and 100% by 2080. This further confirms that by 2080 S_f may probably surpass the historical variability associated with climatological extremes (i.e. 10 warmest winters).

In terms of decline in areal extent of current S_f regions under each warming scenario, GB and SN were most sensitive (Figure 9(a)). For example, spatial extent in GB and SN where S_f is currently greater than 25% may decline under the 2080 warming scenario by 53 ± 9 and $37 \pm 11\%$ of the historical mean, respectively. When this threshold of S_f was increased to 50%, the reduction in spatial extent with respect to the historical mean is even larger (Figure 9(b)). Analysis of areal extent reduction at the regional watershed scale showed very similar patterns (Table 4). By 2080, 35 and 64% of the watersheds where S_f is currently greater than 25 and 50%, respectively, would probably experience a 50–95% reduction in proportional area. As expected, reduction in proportional areal extent is inversely correlated with the watershed average S_f. As noted by Klos *et al.* (2014), loss of currently snow-dominated areas occurred mainly in watersheds with moderate relief and elevation. These types of watersheds are typically warmer and received most precipitation in the form of rain (i.e. lower S_f). In 33 of our 36 study watersheds, reduction in proportional area with $S_f > 50\%$ under the warm winter scenario was higher than those under the 2020 warming scenario. However, was reduced to only five watersheds by 2040, which further confirms warming of 1.8 °C and higher would surpass the historical variability S_f.

As the climate warms, one of the immediate implications from decreasing S_f is a potential increase in winter flooding as the type of precipitation changes from snow to rain. We illustrated this based on historical records that showed flashier streamflow during low as compared with high S_f years (Figure 10). The Richard–Baker flashiness index (Baker *et al.*, 2004) measures oscillations in daily streamflow relative to total streamflow over a time period. Based on 93 USGS stream gage stations (Figure 1(a)), the flashiness index was higher by, on average, 17% during low as compared with high S_f years. These differences are only from the recent period (1950–2003) and may not necessarily reflect the range of stream flashiness over the period of record (1916–2003) for which variability in S_f is presented. Nonetheless, this highlights the strong coupling between the stream hydrograph and type of precipitation (rain or snow) occurring in the entire study region.

4. Discussion and conclusions

This study provides new information on S_f variability and trends across the western United States in a spatially explicit fashion using gridded meteorological data. Our findings reveal underlying geographic patterns in S_f, and provide a foundation for anticipating changes in S_f under

Table 4. Current snow extent (% area with $S_f > 25\%$ and $S_f > 50\%$) and reduction under historical 10 warmest winters (warm winter) and three future warming scenarios (i.e. 2020, 2040, and 2080).

HUC4 watershed	Current proportional area (%)	Reduction in proportional area (%)				Current proportional area (%)	Reduction in proportional area (%)			
		Warm winter	2020	2040	2080		Warm winter	2020	2040	2080
	$S_f > 25\%$					$S_f > 50\%$				
Bear	100 (0)	8 (4)	1 (2)	3 (3)	8 (4)	91 (0)	12 (4)	6 (2)	11 (3)	25 (4)
Black Rock Desert-Humboldt	96 (7)	30 (12)	10 (6)	19 (8)	38 (13)	61 (7)	57 (12)	34 (6)	55 (8)	80 (13)
Central Lahontan	89 (14)	48 (10)	21 (11)	36 (12)	57 (9)	42 (14)	46 (10)	32 (11)	48 (12)	69 (9)
Central Nevada Desert Basins	86 (5)	29 (11)	9 (5)	17 (8)	35 (11)	56 (5)	52 (11)	30 (5)	49 (8)	76 (11)
Colorado Headwaters	100 (0)	2 (2)	0 (1)	1 (2)	5 (4)	94 (0)	7 (2)	5 (1)	9 (2)	16 (4)
Escalante Desert-Sevier Lake	99 (2)	23 (16)	5 (8)	13 (14)	33 (17)	63 (2)	37 (16)	27 (8)	40 (14)	60 (17)
Great Divide-Upper Green	100 (0)	0 (0)	0 (0)	0 (0)	0 (0)	100 (0)	0 (0)	0 (0)	1 (0)	6 (0)
Great Salt Lake	95 (8)	34 (12)	12 (10)	24 (12)	43 (10)	52 (8)	44 (12)	28 (10)	45 (12)	69 (10)
Gunnison	100 (0)	3 (3)	1 (2)	2 (3)	6 (4)	93 (0)	6 (3)	4 (2)	7 (3)	12 (4)
Klamath-Northern California Coastal	53 (8)	41 (18)	22 (11)	38 (16)	66 (15)	26 (8)	62 (18)	50 (11)	70 (16)	89 (15)
Kootenai-Pend Oreille-Spokane	99 (1)	3 (3)	2 (3)	5 (4)	12 (4)	90 (1)	9 (3)	10 (3)	18 (4)	33 (4)
Little Colorado	75 (13)	33 (8)	21 (5)	34 (8)	58 (11)	35 (13)	59 (8)	50 (5)	72 (8)	92 (11)
Lower Colorado-Lake Mead	52 (10)	48 (12)	25 (7)	41 (9)	63 (7)	22 (10)	51 (12)	39 (7)	56 (9)	78 (7)
Lower Columbia	38 (9)	31 (6)	27 (5)	41 (5)	64 (8)	21 (9)	43 (6)	36 (5)	55 (5)	82 (8)
Lower Green	100 (1)	6 (5)	2 (3)	5 (4)	11 (5)	83 (1)	23 (5)	13 (3)	23 (4)	37 (5)
Lower Snake	90 (5)	11 (3)	7 (3)	13 (4)	23 (4)	73 (5)	13 (3)	12 (3)	18 (4)	31 (4)
Middle Columbia	77 (12)	30 (11)	20 (6)	34 (9)	58 (12)	37 (12)	56 (11)	43 (6)	64 (9)	85 (12)
Middle Snake	96 (5)	16 (7)	6 (3)	11 (4)	24 (10)	73 (5)	39 (7)	24 (3)	41 (4)	65 (10)
North Lahontan	91 (10)	41 (15)	15 (8)	29 (12)	55 (17)	51 (10)	67 (15)	47 (8)	70 (12)	91 (17)
Northern Mojave-Mono Lake	31 (5)	36 (2)	19 (2)	30 (2)	45 (2)	18 (5)	28 (2)	20 (2)	30 (2)	46 (2)
Oregon Closed Basins	100 (1)	20 (19)	3 (6)	10 (13)	31 (24)	70 (1)	68 (19)	44 (6)	66 (13)	89 (24)
Oregon-Washington Coastal	17 (6)	40 (5)	32 (4)	45 (5)	63 (3)	8 (6)	37 (5)	31 (4)	48 (5)	73 (3)
Puget Sound	40 (5)	17 (3)	16 (3)	26 (4)	42 (4)	29 (5)	20 (3)	20 (3)	32 (4)	50 (4)
Sacramento	46 (6)	39 (16)	19 (10)	34 (14)	61 (15)	25 (6)	57 (16)	46 (10)	66 (14)	86 (15)
Salt	39 (12)	50 (3)	33 (5)	50 (4)	69 (3)	15 (12)	50 (3)	39 (5)	58 (4)	83 (3)
San Joaquin	29 (2)	12 (3)	7 (2)	12 (3)	21 (2)	25 (2)	12 (3)	10 (2)	15 (3)	25 (2)
San Juan	95 (7)	20 (14)	13 (10)	25 (15)	50 (17)	49 (7)	39 (14)	38 (10)	53 (15)	69 (17)
Tulare-Buena Vista Lakes	27 (3)	19 (2)	11 (2)	18 (2)	28 (2)	21 (3)	15 (2)	11 (2)	17 (2)	28 (2)
Upper Colorado-Dirty Devil	89 (7)	25 (12)	12 (6)	22 (10)	42 (11)	52 (7)	36 (12)	28 (6)	40 (10)	55 (11)
Upper Colorado-Dolores	97 (5)	16 (7)	7 (5)	13 (6)	26 (9)	69 (5)	26 (7)	20 (5)	32 (6)	50 (9)
Upper Columbia	97 (2)	9 (6)	5 (4)	9 (6)	20 (7)	77 (2)	15 (6)	13 (4)	21 (6)	35 (7)
Upper Gila	30 (6)	29 (7)	22 (2)	35 (5)	59 (13)	14 (6)	57 (7)	54 (2)	76 (5)	95 (13)
Upper Snake	98 (2)	9 (4)	3 (2)	6 (2)	13 (3)	85 (2)	24 (4)	12 (2)	21 (2)	37 (3)
White-Yampa	100 (0)	0 (0)	0 (0)	0 (0)	0 (1)	98 (0)	9 (0)	6 (0)	12 (0)	29 (1)
Willamette	33 (7)	33 (9)	25 (7)	40 (11)	66 (11)	18 (7)	53 (9)	44 (7)	65 (11)	86 (11)
Yakima	96 (6)	17 (11)	9 (7)	18 (10)	38 (14)	60 (6)	31 (11)	28 (7)	45 (10)	71 (14)

Parenthetical values are one standard deviation and express variability in the estimates due to the plausible range of TR (−1 to +4 °C) and TS (−2 to 0 °C) threshold values ($n = 49$).

climate warming at a daily resolution. Consistent with previous analyses (i.e. Knowles *et al.*, 2006; Das *et al.*, 2009; Serquet *et al.*, 2011), we show that winter temperature, as opposed to precipitation variability, is the primary control on S_f. The difference in S_f between cold and warm winters during 1916–2003 at low- and mid-elevations has ranged between 31% in the PNW to as much as 40% in the SN. In contrast, the difference in S_f between wet and dry winters during 1916–2003 at all elevation ranges is not significantly different across all four regions. Interestingly, the majority of the 10 wettest (at least 7 of 10) and warmest (at least 8 of 10) winters during the period 1916–2003 occur post 1950s.

We illustrate a high sensitivity of S_f under average wet daily temperature values (November–March) between 5 and −5 °C. In the Northern Sierra, Klamath Mountains, and western slopes of the Cascade Mountain Range, a 1 °C increase in winter temperature would result in a decrease

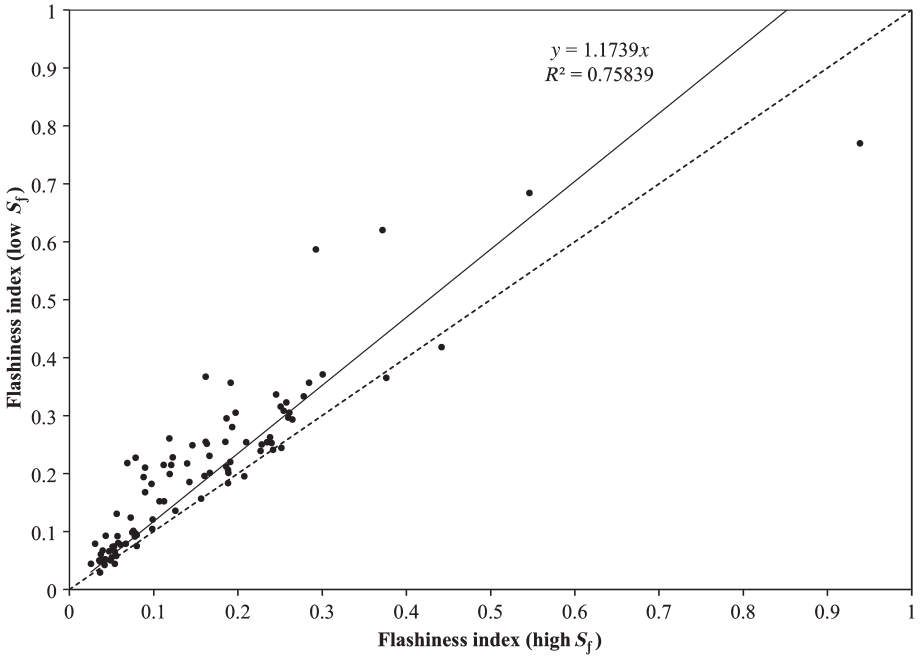

Figure 10. Comparisons of January–March Richard–Baker flashiness index (Baker *et al.*, 2004) between low (**10th** percentile) and high (**90th** percentile) S_f years at 93 USGS gages during 1950–2003, with linear fit (solid line) and 1 : 1 line (dashed line).

of 10–15% in S_f. Although our results further confirm a significant decline in S_f across the entire region we show that this reduction is more pronounced during the recent decades (1960–2003) as compared with the longer historical period (1916–2003). There has also been a recent (1960–2003) regional shift in S_f trends and SNR. The warming scenario analysis indicates that natural variability in S_f over 1916–2003 most closely resembles the 2040 warming scenario, except for the GB region. This suggests that under the future scenarios examined here, the long-term trend in S_f (with inter-annual variability removed) would begin to exceed the historical range of S_f variability around 2040, corresponding here to a warming of 1.8 °C relative to historical temperature. In addition, we demonstrated a differential decline in S_f across the four geographic units SN, CRB, GB, and PNW indicating a non-homogenous effect of the recent (1960–2003) warming climate across the region.

Our trend analysis approach yields S_f sensitivities that are in agreement with those reported by Nolin and Daly (2006), and expands this sensitivity mapping to include geographies with lower S_f sensitivity. However, the high S_f sensitivity regions show a strong SNR indicating that the trend in S_f has already exceeded the historical variability. Given that many of the high S_f sensitivity regions fall in the mid-elevation range, a continued warming climate (Mote and Salathé, 2010) would push future S_f even further outside its historical variability. Our warming scenarios also show significant shifts in S_f across the four regions, some more than others. The actual magnitude and changes in S_f presented in this study are subjected to uncertainties; especially at lower elevations where agreement between empirically derived S_f and those measured at SNOTEL sites were poor. Uncertainties associated with temperature threshold-based S_f portioning, however, are far smaller than the projected change in S_f and corresponding snow extent areal reduction; giving confidence in the results. Also, uniform increases of 1.1, 1.8, and 3.0 °C may not accurately represent the uncertainties associated with future warming that could vary in both space and time. Nonetheless, this simplistic approach provides a relative comparison of future S_f in terms of sensitivity to temperature across the region. Our findings also imply that uncertainties associated with future changes in precipitation, which show mixed trends across the domain (Dominguez *et al.*, 2012; Reclamation, 2013) and strong disagreement between new-generation CMIP5 and old-generation CMIP3 models (Reclamation, 2013), should not affect temperature-driven S_f sensitivity.

Runoff from mountain snowmelt is the primary source of water in much of the western United States. A decline in S_f would increase winter runoff, reduce snowpack, and subsequently reduce summer runoff, with widespread implications for water management, including reservoir operations (Barnett and Pierce, 2009; Brekke *et al.*, 2009; Danner, 2013) and irrigation regimes (Benson and Williams, 2013; McDonald and Girvetz, 2013). In addition to a seasonal shift in the timing and magnitude of streamflow (Barnett *et al.*, 2005; Regonda *et al.*, 2005; Stewart *et al.*, 2005; Luce and Holden, 2009), decline in S_f is likely to reduce total annual streamflow. A recent study by Berghuijs *et al.* (2014) reports a significant linear increase in precipitation-normalized streamflow of $0.37/U^{-1}$ increase in S_f. We show that a warming of only 1.8 °C under the 2040 scenario would result in a S_f lower than the warm winters during the period 1916–2003, and may require changing the way water infrastructure is currently managed (Danner, 2013).

References

Abatzoglou JT. 2011. Influence of the PNA on declining mountain snowpack in the western United States. *Int. J. Climatol.* **31**(8): 1135–1142.

Abatzoglou JT, Rupp DE, Mote PW. 2014. Seasonal climate variability and change in the Pacific Northwest of the United States. *J. Clim.* **27**(5): 2125–2142.

Adam JC, Hamlet AF, Lettenmaier DP. 2009. Implications of global climate change for snowmelt hydrology in the twenty-first century. *Hydrol. Process.* **23**(7): 962–972.

Baker DB, Richards RP, Loftus TT, Kramer JW. 2004. A new flashiness index: characteristics and applications to Midwestern Rivers and streams. *J. Am. Water Resour. Assoc.* **40**(2): 503–522.

Barnett TP, Pierce DW. 2009. Sustainable water deliveries from the Colorado River in a changing climate. *Proc. Natl. Acad. Sci. U. S. A.* **106**(18): 7334–7338.

Barnett TP, Adam JC, Lettenmaier DP. 2005. Potential impacts of a warming climate on water availability in snow-dominated regions. *Nature* **438**: 303–309.

Barnett TP, Pierce DW, Hidalgo HG, Bonfils C, Santer BD, Das T, Bala G, Wood AW, Nozawa T, Mirin AA, Cayan DR, Dettinger MD. 2008. Human-induced changes in the hydrology of the western United States. *Science* **319**(5866): 1080–1083.

Benson A, Williams R. 2013. Cost of early snowmelt in terms of reduced irrigation deliveries. *J. Nat. Resour Policy Res.* **5**(2–3): 79–89.

Berghuijs WR, Woods RA, Hrachowitz M. 2014. A precipitation shift from snow towards rain leads to a decrease in streamflow. *Nat. Clim. Change* **4**(7): 583–586.

Brekke LD, Maurer EP, Anderson JD, Dettinger MD, Townsley ES, Harrison A, Pruitt T. 2009. Assessing reservoir operations risk under climate change. *Water Resources Research* **45**: W04411, doi: 10.1029/2008WR006941.

Brown RD, Mote PW. 2009. The response of northern hemisphere snow cover to a changing climate. *J. Clim.* **22**(8): 2124–2145.

Christner J, Harr RD. 1982. Peak streamflows from the transient snow zone, Western Cascades, Oregon. In *50th Annual Meeting Western Snow Conference*, Harr RD (ed). Colorado State University: Reno, NV.

Dai A. 2008. Temperature and pressure dependence of the rain-snow phase transition over land and ocean. *Geophys. Res. Lett.* **35**: L12802, doi: 10.1029/2008GL033295.

Danner AG. 2013. *Will We Need to Change the Rules: Assessing the Implications of Climate Change for Dam Operations in Oregon's McKenzie River Basin*. MS thesis, Oregon State University: Corvallis, Oregon.

Das T, Hidalgo HG, Pierce DW, Barnett TP, Dettinger MD, Cayan DR, Bonfils C, Bala G, Mirin A. 2009. Structure and detectability of trends in hydrological measures over the western United States. *J. Hydrometeorol.* **10**(4): 871–892.

Déry SJ, Mlynowski TJ, Hernández-Henríquez MA, Straneo F. 2011. Interannual variability and interdecadal trends in Hudson Bay streamflow. *J. Mar. Syst.* **88**(3): 341–351.

Dettinger MD, Cayan DR, Meyer MK, Jeton AE. 2004. Simulated hydrologic responses to climate variations and change in the Merced, Carson, and American River basins, Sierra Nevada, California, 1900–2099. *Clim. Change* **62**(1–3): 283–317.

Dominguez F, Rivera E, Lettenmaier D, Castro C. 2012. Changes in winter precipitation extremes for the western United States under a warmer climate as simulated by regional climate models. *Geophys. Res. Lett.* **39**(5): L05803.

Feng S, Hu Q. 2007. Changes in winter snowfall/precipitation ratio in the contiguous United States. *J. Geophys. Res.* **112**: D15109, doi: 10.1029/2007JD008397.

Ficklin DL, Barnhart BL, Knouft JH, Stewart IT, Maurer EP, Letsinger SL, Whittaker GW. 2014. Climate change and stream temperature projections in the Columbia River basin: habitat implications of spatial variation in hydrologic drivers. *Hydrol. Earth Syst. Sci.* **18**(12): 4897–4912.

Frei A, Robinson DA, Hughes MG. 1999. North American snow extent: 1900–1994. *Int. J. Climatol.* **19**(14): 1517–1534.

Gleick PH. 1987. Regional hydrologic consequences of increases in atmospheric CO_2 and other trace gases. *Clim. Change* **10**(2): 137–160.

Hamlet AF, Lettenmaier DP. 2005. Production of temporally consistent gridded precipitation and temperature fields for the continental United States. *J. Hydrometeorol.* **6**(3): 330–336.

Hamlet AF, Lettenmaier DP. 2007. Effects of 20th century warming and climate variability on flood risk in the western U.S. *Water Resour. Res.* **43**: W06427, doi: 10.1029/2006WR005099.

Hamlet AF, Mote PW, Clark MP, Lettenmaier DP. 2005. Effects of temperature and precipitation variability on snowpack trends in the Western United States. *J. Clim.* **18**(21): 4545–4561.

Harpold A, Brooks P, Rajagopal S, Heidbuchel I, Jardine A, Stielstra C. 2012. Changes in snowpack accumulation and ablation in the intermountain west. *Water Resour. Res.* **48**: W11501, doi: 10.1029/2012WR011949.

Harr RD. 1981. Some characteristics and consequences of snowmelt during rainfall in western Oregon. *J. Hydrol.* **53**(3): 277–304.

Harr RD. 1986. Effects of clearcutting on rain on snow runoff in Western Oregon: a new look at old studies. *Water Resour. Res.* **22**: 383–392.

Hay LE, Wilby RL, Leavesley GH. 2000. A comparison of delta change and downscaled GCM scenarios for three mountainous basins in the United States. *J. Am. Water Resour. Assoc.* **36**(2): 387–397.

Hidalgo HG, Das T, Dettinger MD, Cayan DR, Pierce DW, Barnett TP, Bala G, Mirin A, Wood AW, Bonfils C, Santer BD, Nozawa T. 2009. Detection and attribution of streamflow timing changes to climate change in the Western United States. *J. Clim.* **22**(13): 3838–3855.

Intergovernmental Panel on Climate Change (IPCC), 2007a. Summary for policymakers. In *Climate Change 2007: The Physical Science Basis. Contribution of Working Group I to the Fourth Assessment Report of the Intergovernmental Panel on Climate Change*, Solomon S, Qin D, Manning M, Chen Z, Marquis M, Averyt KB, Tignor M, Miller HL (eds). Cambridge University Press: Cambridge, UK and New York, NY.

Intergovernmental Panel on Climate Change (IPCC). 2007b. *Climate Change 2007: Impacts, Adaptation And Vulnerability*. Contribution of Working Group II to the Fourth Assessment Report of the Intergovernmental Panel on Climate Change, Parry ML, Canziani OF, Palutikof JP, van der Linden PJ, Hanson CE (eds). Cambridge University Press: Cambridge, UK and Geneva, Switzerland, 976 pp.

Jefferson AJ. 2011. Seasonal versus transient snow and the elevation dependence of climate sensitivity in maritime mountainous regions. *Geophys. Res. Lett.* **38**: L16402, doi: 10.1029/2011GL048346.

Karl TR, Jones PD, Knight RW, Kukla G, Plummer N, Razuvayev V, Gallo KP, Lindseay J, Charlson RJ, Peterson TC. 1993. Asymmetric trends of daily maximum and minimum temperature. *Bull. Am. Meteorol. Soc.* **74**(6): 1007–1023.

Kendall MG. 1938. A new measure of rank correlation. *Biometrika* **30**(1/2): 81–93.

Klos PZ, Link TE, Abatzoglou JT. 2014. Extent of the rain-snow transition zone in the western U.S. under historic and projected climate. *Geophys. Res. Lett.* **41**: 4560–4568, doi: 10.1002/2014GL060500.

Knowles N, Cayan DR. 2004. Elevational dependence of projected hydrologic changes in the San Francisco estuary and watershed. *Clim. Change* **62**(1–3): 319–336.

Knowles N, Dettinger MD, Cayan DR. 2006. Trends in snowfall versus rainfall in the Western United States. *J. Clim.* **19**: 4545–4559.

Lettenmaier DP, Gan TY. 1990. Hydrologic sensitivities of the Sacramento-San Joaquin River Basin, California, to global warming. *Water Resour. Res.* **26**(1): 69–86.

Lins HF, Slack JR. 1999. Streamflow trends in the United States. *Geophys. Res. Lett.* **26**(2): 227–230.

Luce CH, Holden ZA. 2009. Declining annual streamflow distributions in the Pacific Northwest United States, 1948–2006. *Geophys. Res. Lett.* **36**: L16401, doi: 10.1029/2009GL039407.

Mao Y, Nijssen B, Lettenmaier DP. 2015. Is climate change implicated in the 2013–2014 California drought? A hydrologic perspective. *Geophys. Res. Lett.* **42**: 2805–2813, doi: 10.1002/2015GL063456.

Marks D, Kimball J, Tingey D, Link T. 1998. The sensitivity of snowmelt processes to climate conditions and forest cover during rain on snow: a case study of the 1996 Pacific Northwest flood. *Hydrol. Process.* **12**: 1569–1587.

McDonald RI, Girvetz EH. 2013. Two challenges for US irrigation due to climate change: increasing irrigated area in wet states and increasing irrigation rates in dry states. *PLoS One* **8**(6): e65589.

Mehran A, AghaKouchak A, Phillips TJ. 2014. Evaluation of CMIP5 continental precipitation simulations relative to satellite-based gauge-adjusted observations. *J. Geophys. Res.-Atmos.* **119**(4): 1695–1707.

Mishra V, Cherkauer KA. 2011. Influence of cold season climate variability on lakes and wetlands in the Great Lakes region. *J. Geophys. Res.-Atmos.* **116**: D12111, doi: 10.1029/2010JD015063.

Mote, P. and Salathé, E., 2009. Future climate in the Pacific Northwest (Chapter 1). In *The Washington Climate Change Impacts Assessment*, Elsner MM, Littell J, Binder LW (eds). Center for Science in the Earth System, Joint Institute for the Study of the Atmosphere and Oceans, University of Washington: Seattle,

WA. http://www.cses.washington.edu/db/pdf/wacciareport681.pdf (accessed 23 October 2015).
Mote PW, Salathé EP. 2010. Future climate in the Pacific Northwest. *Clim. Change* **102**(1–2): 29–50.
Mote PW, Hamlet AF, Clark MP, Lettenmaier DP. 2005. Declining mountain snowpack in Western North America. *Bull. Am. Meteorol. Soc.* **86**(1): 39–49.
Nolin AW, Daly C. 2006. Mapping "at risk" snow in the Pacific Northwest. *J. Hydrometeorol.* **7**: 1164–1171.
O'Connor JE, Costa JE. 2003. Large floods in the United States: where they happen and why. Circular 1245. US Geological Survey, Reston, VA.
Reclamation. 2013. Downscaled CMIP3 and CMIP5 climate and hydrology projections: release of downscaled CMIP5 climate projections, comparison with preceding information, and summary of user needs, prepared by the U.S. Department of the Interior, Bureau of Reclamation, Technical Services Center, Denver, CO, 47 pp.
Regonda SK, Rajagopalan B, Clark M, Pitlick J. 2005. Seasonal cycle shifts in hydroclimatology over the western US. *J. Clim.* **18**: 372–384.
Rupp DE, Mote PW, Bindoff NL, Stott PA, Robinson DA. 2013. Detection and attribution of observed changes in Northern Hemisphere spring snow cover. *J. Clim.* **26**(18): 6904–6914.
Safeeq M, Grant G, Lewis S, Tague C. 2013. Coupling Snowpack and groundwater dynamics to interpret historical streamflow trends in the Western United States. *Hydrol. Process.* **27**(5): 655–668.
Safeeq M, Grant GE, Lewis SL, Staab B. 2015. Predicting landscape sensitivity to present and future floods in the Pacific Northwest, USA. *Hydrol. Process.*, doi: 10.1002/hyp.10553.
Sen PK. 1968. Estimates of the regression coefficient based on Kendall's tau. *J. Am. Stat. Assoc.* **63**(324): 1379–1389.
Serquet G, Marty C, Dulex JP, Rebetez M. 2011. Seasonal trends and temperature dependence of the snowfall/precipitation-day ratio in Switzerland. *Geophys. Res. Lett.* **38**: L07703, doi: 10.1029/2011GL046976.
Shukla S, Safeeq M, AghaKouchak A, Guan K, Funk C. 2015. Temperature impacts on the water year 2014 drought in California. *Geophys. Res. Lett.* **42**(11): 4384–4393.
Sproles E, Nolin A, Rittger K, Painter T. 2013. Climate change impacts on maritime mountain snowpack in the Oregon Cascades. *Hydrol. Earth Syst. Sci.* **17**(7): 2581–2597.
Stewart IT, Cayan DR, Dettinger MD. 2004. Changes in snowmelt runoff timing in western North America under a business as usual climate change scenario. *Clim. Change* **62**(1–3): 217–232.
Stewart I, Cayan DR, Dettinger M. 2005. Changes toward earlier streamflow timing across western North America. *J. Clim.* **18**: 1136–1155.
Surfleet CG, Tullos D. 2012. Variability in effect of climate change on rain on snow peak flow events in a temperate climate. *J. Hydrol.* **479**: 24–34.
U.S. Army Corps of Engineers. 1956. Snow hydrology; Summary report of snow investigations. U.S. Department of Commerce Office of Technical Services, Washington, D.C., 437 pp.

